Structure of Monolayers of Monododecyl Dodecaethylene Glycol at the Air−Water Interface Studied by Neutron Reflection

J. R. Lu* and T. J. Su

Department of Chemistry, University of Surrey, Guildford GU2 5XH, UK

Z. X. Li and R. K. Thomas

Physical and Theoretical Chemistry Laboratory, South Parks Road, Oxford OX1 3QZ, UK

E. J. Staples and I. Tucker

Unilever Research, Port Sunlight Laboratory, Quarry Road East, Wirral, L63 3JW, UK

J. Penfold

ISIS, CCLRC, Chilton, Didcot OX11 0QX, UK

Received: April 17, 1997; In Final Form: September 18, 1997[⊗]

We have determined the structure of a monolayer of dodecaethylene glycol monododecyl ether ($C_{12}E_{12}$) adsorbed at the air−water interface using specular neutron reflection in combination with deuterium labeling. The structure of the adsorbed monolayer was measured at its critical micellar concentration (cmc, 1.25×10^{-4} M), 0.3cmc, 0.13cmc, and 0.033cmc. The reflection data were analyzed using the optical matrix method and the kinematic approximation, both of which gave structures identical within the limitations of the different models used. In the optical matrix method the monolayer was divided into two layers, the first layer consisting of the alkyl chain only, and the second layer consisting of the ethoxylated head, a fraction of the alkyl chain, and water. Significant intermixing of alkyl chain and ethoxylated headgroup was needed to account for the observed reflectivities. At the cmc about 35% of the alkyl chain seems to be incorporated into the headgroup region, and this increases to about 50% at the lowest concentration. The corresponding variation in the thickness of the alkyl chain layer was from 9 to 6 ± 2 Å and that of the head region from 22 to 20 ± 2 Å. The distances between the centers of the alkyl chain and solvent distributions were determined by the more direct kinematic method and the values were found to be 13, 11, 10, and 7.5 ± 2 Å for the four concentrations studied. The total thicknesses of the dodecyl chain and the ethoxylate groups were extracted from a simultaneous analysis of three reflectivity profiles from different isotopic compositions at a given surfactant concentration. The values of the two thicknesses were found to be 15.0, 13.0, 12.5, and 12.0 ± 2 Å for the dodecyl chain and 21, 18, 17, and 17 ± 4 Å for the ethoxylate group at the four concentrations. Comparison of these values with previous work on $C_{12}E_n$ with shorter ethylene glycol chains shows that the distributions of the dodecyl chain are similar to those with smaller *n*, but the extent of mixing between the alkyl chain and the ethoxylate group increases with *n*.

Introduction

Nonionic surfactants of alkyl ethoxylates (C_mE_n) are widely used in detergency, cosmetics, shampoo, paints, pharmacy, and fabric softening. Most of these applications rely on properties associated with either interfacial adsorption or aggregation in solution. Much has been published on their phase diagrams, their interactions with polymers, and their aggregation behavior, but little is known about the structure of their monolayers at planar interfaces. The molecular conformation of a surfactant is bound to influence its interfacial and aggregation behavior, and the relation between chemical architecture and surface activity is vital for understanding surfactant function. For example, the geometrical approach to aggregate structure which essentially uses headgroup areas as an adjustable parameter[1] gives an effective description of the general phase behavior of surfactants, but it needs to be extended by direct structural measurement, otherwise it may give misleading conclusions. An example is the description of the temperature-induced phase inversion of microemulsions containing nonionic surfactants.[2] That the situation is more complex than the usual simple picture is shown by recent neutron reflection measurements which indicate that there may be significant intermixing of alkyl chains and ethoxylated headgroups inside nonionic surfactant monolayers.[3] The stiffness of the two chains, the variation in their conformations and the dehydration of the ethylene oxide groups with increase of temperature, and the surface roughness must all play a contributory role. Our previous studies of the $C_{12}E_n$ surfactants[3−6] have indicated that the fragments of the surfactant where the hydrophobic and hydrophilic groups join is more tilted than the outer part of the alkyl chain in the surface monolayer, giving the alkyl chain a conformation somewhat different from that of the cationic alkyl trimethylammonium bromide surfactants.[7,8] As a part of systematic study of the series of $C_{12}E_n$, we here report a study of the structure of $C_{12}E_{12}$ at the air−water interface. One of the main purposes of the present study is to examine the gradual change in monolayer structure and composition with the length of the headgroup and to monitor the evolution of the headgroup distribution as it becomes more polymer-like.[9]

[⊗] Abstract published in *Advance ACS Abstracts,* November 15, 1997.

S1089-5647(97)01330-8 CCC: $14.00

Experimental Section

Two isotopic species of the surfactant were synthesized, $C_{12}D_{25}(OC_2H_4)_{12}OH$ and $C_{12}H_{25}(OC_2H_4)_{12}OH$, abbreviated as $dC_{12}hE_{12}$ and $hC_{12}hE_{12}$, respectively. $hC_{12}hE_{12}$ was prepared by reacting $hC_{12}hE_6$ (Fluka, 99%) with hexaethylene glycol (Fluka, 99%). The synthetic route was similar to that of Booth et al.[10] A pure sample of $hC_{12}hE_6$ (2 g, 4.5×10^{-3} mol) was dried on a vacuum line, and to it was added dry dichloromethane (10 mL) as solvent, *p*-toluenesulfonyl chloride (Fluka, 99%) (0.85 g, 4.5×10^{-3} mol), and dry triethylamine (0.5 g, 5×10^{-3} mol). The reaction vessel was cooled in ice during this process. The stirred reaction was left overnight. The triethylamine hydrochloride was filtered off and the dichloromethane phase washed with water to remove any dissolved inorganic salt. The solvent was evaporated on a rotary evaporator and the remaining oily sample dried on a vacuum line overnight. In a separate flask hexaethylene glycol (5 g, 1.8×10^{-2} mol) was dried overnight with stirring at 40 °C. Potassium *tert*-butoxide (0.55 g, 4.5×10^{-3} mol) was introduced, and when the reaction was complete, the sample was mixed with the $C_{12}E$-tosylate. The mixture was stirred and heated at 70 °C for 2 h. About 10 mL of boiling water was then added to the mixture, and stirring continued for another hour. When cool, the solution was neutralized with HCl and extracted with ether. Evaporation of the solvent left a light yellow oil which was purified by flash chromatography on a silica column. Alkyl chain deuterated $dC_{12}hE_{12}$ was synthesized following a similar procedure as described above. $dC_{12}hE_6$ was made by the Williamson reaction from the deuterated dodecyl bromide, an equimolar amount of sodium, and a 5-fold molar excess of hexaethylene glycol.[4] Deuterated dodecyl bromide was purchased from K&K Greeff, UK, and over 98% H in the dodecyl chain has been converted into D.

The neutron reflection measurements were made on the white beam reflectometer SURF at the Rutherford-Appleton Laboratory, ISIS, Didcot, UK.[11] The procedure for performing the measurements has been described previously.[12] Surfactant solutions were poured into a Teflon trough to give a positive liquid meniscus. The trough was mounted on an antivibration bench. Beam intensities were calibrated with respect to D_2O. A flat background determined by extrapolation to the high values of momentum transfer, κ ($\kappa = (4\pi \sin \theta)/\lambda$) where λ is the wavelength and θ is the glancing angle of incidence, was subtracted. All the experiments were performed at 25 °C. High-purity water was used for all the measurements (Elga Ultrapure), and all the glassware and Teflon troughs for the reflection measurements were cleaned using alkaline detergent (Decon 90) followed by repeated washing in ultrapure water. Surface tension measurements were made using a Kruss K10 maximum pull tensiometer with a Pt du Nouy ring. For a given concentration three readings were typically taken, and the difference between the repeated measurements was usually less than 0.5 mN m^{-1} around the critical micellar concentration (cmc) and was about 1 mN m^{-1} over the dilute concentration region. The points measured below the cmc were fitted to a second-order polynomial curve which was combined with the Gibbs equation to obtain area per molecule.

Theory

Neutron reflectivities can be analyzed using the optical matrix method or the kinematic approximation. A detailed description of the optical matrix method for calculating neutron reflectivities has been given by Born and Wolf[13] and Lekner.[14] The procedure for extracting structural information from experimental profiles is straightforward. A structural model is assumed and the exact reflectivity calculated using the optical matrix formula. The calculated reflectivity is then compared with the measured one and the structural parameters modified in a least-squares iteration. The parameters used in the calculation are mainly the thickness of the layers, τ, and the corresponding scattering length densities, ρ, which depend on the number densities of each atom species, n_i, and their known scattering lengths, b_i:

$$\rho = \sum n_i b_i \tag{1}$$

The use of isotopic labeling can provide a set of different reflectivity profiles for a given chemical structure. Since the scattering length density of a given layer varies with isotopic composition, the fitting of a set of isotopic compositions to a single structural model greatly increases the certainty of the interpretation, although it adds to the complexity of the fitting procedure. Deuterium/hydrogen substitution is particularly useful for surfactants and polymers. Since the scattering lengths of D and H are of opposite sign, the scattering length density of water can be varied over a wide range. The simplest example is water made by mixing 1 mol of D_2O with 9 mol of H_2O (null reflecting water, NRW). When a deuterated surfactant is adsorbed at the air−water interface of NRW, the surfactant is the only species that contributes to the specular reflectivity. Under this condition, if the adsorbed layer is assumed to be uniform, the area per molecule, A, is given by

$$A = \sum n_i b_i / \rho\tau \tag{2}$$

In fitting the reflectivity profiles with a uniform layer model, it is usually found that τ and ρ can be varied over a limited range, but the variations cancel in their contribution to A so that A is to a good approximation independent of the assumption that the layer is uniform. The kinematic approach can allow a more realistic description of the structure of the different components constituting the interface.[15,16] In this approximation the reflectivity, $R(\kappa)$, is given by

$$R(\kappa) = (16\pi^2/\kappa^4)|\rho'(\kappa)|^2 \tag{3}$$

where $\rho'(\kappa) = \kappa^2\rho(\kappa)$. $\rho(\kappa)$ is the one-dimensional Fourier transform of $\rho(z)$, the average scattering length density profile in the direction normal to the surface

$$\rho'(\kappa) = \int_{-\infty}^{\infty} \kappa^2 \exp(-i\kappa z)\rho(\kappa)\, dz \tag{4}$$

In terms of the distributions from different components in the monolayer of $C_{12}E_{12}$, the scattering length density profile can be written as

$$\rho(\kappa) = b_c n_c(z) + b_h n_h(z) + b_w n_w(z) \tag{5}$$

where c, h, and w refer to surfactant chains, ethoxylated headgroups, and water. Substituting (5) into (4) and (3) gives

$$R(\kappa) = (16\pi^2/\kappa^2)[b_c^2 h_{cc}(\kappa) + b_h^2 h_{hh}(\kappa) + b_w^2 h_{ww}(\kappa) + 2b_c b_h h_{ch}(\kappa) + 2b_c b_w h_{cw}(\kappa) + 2b_h b_w h_{hw}(\kappa)] \tag{6}$$

where $h_{ii}(\kappa)$ and $h_{ij}(\kappa)$ are the partial structure factors. The relationship between the partial structure factors and number density distribution functions are

$$h_{ii}(\kappa) = |\hat{n}_i(\kappa)|^2 \tag{7}$$

$$h_{ij}(\kappa) = \mathrm{Re}|\hat{n}_i(\kappa)\, \hat{n}_j(\kappa)| \tag{8}$$

where $\hat{n}_i(\kappa)$ or $\hat{n}_j(\kappa)$ is the one-dimensional Fourier transform of the appropriate number density and can be obtained from an equation similar to (4). If the number density distributions corresponding to the two self-structure factors h_{ii} and h_{jj} are symmetrical, the relative distance between the centers of the two distributions can be determined through the cross term in the structure factor

$$h_{ij}(\kappa) = \pm\sqrt{h_{ii}h_{jj}}\cos(\kappa\delta_{ij}) \tag{9}$$

where δ_{ij} is the distance between the centers of the two distributions. If one distribution is even and the other is odd, then

$$h_{ij}(\kappa) = \pm\sqrt{h_{ii}h_{jj}}\sin(\kappa\delta_{ij}) \tag{10}$$

The distributions of surfactants and their fragments across the interface approximate closely to these two limits. Thus, eqs 9 and 10 offer a route for determining the separation between pairs of distributions without either Fourier transformation or specific assumptions about the type of distribution apart from its being even or old.

The choice of the optimum route for deriving number density distributions from self-partial structure factors is less straightforward. In principle, number density distributions can be obtained directly by Fourier transformation, but in practice the errors are too large because of the limited range of momentum transfer over which the data are measured. At present, reflectivities can only be measured up to relatively low momentum transfers because of the significant background from incoherent scattering. The use of suitable analytic expressions for the partial structure factors is therefore a more convenient approach. A simple and appropriate model to represent a soluble surfactant monolayer is a Gaussian distribution

$$n_i(z) = n_0\exp(-4z^2/\sigma^2) \tag{11}$$

where n_i denotes the number density distribution, n_0 is the number density at the center of the distribution, and σ is the full width at n_0/e. Substitution of (11) into (4) and (7) gives

$$h_{ii}(\kappa) = \Gamma^2\exp(-\sigma^2\kappa^2/8) \tag{12}$$

where Γ is the surface excess and is equal to $\sqrt{\pi}\sigma n_0/2$. The distributions of the alkyl chain, the head, and the whole molecule are each fairly symmetrical and are expected to be quite well described by eq 11. For the water distribution across the interfacial region a tanh function has been found to be suitable

$$h_{ww}(\kappa) = {n_0}^2(\pi\xi/2)^2\,\mathrm{csch}^2(\pi\xi\kappa/2) \tag{13}$$

where ξ is the width parameter of the tanh function.

Results and Discussion

Surface tension measurements were used to check the purity of the two samples and to determine the critical micellar concentration (cmc). The absence of a minimum around the cmc indicates that the samples prepared were of high purity. Figure 1 shows the variation of surface tension with log-[concentration] for the fully hydrogenated surfactant. The cmc was found to be $(1.25 \pm 0.2) \times 10^{-4}$ M, compared with 1.4×10^{-4} M obtained by Lange using the same method.[17] The surface tension plot for $dC_{12}hE_{12}$ was found to be identical with that for $hC_{12}hE_{12}$ within an error of 0.5 mN m^{-1} over the same concentration range. The agreement was better around the cmc, suggesting that both surfactants were of high purity. Analysis

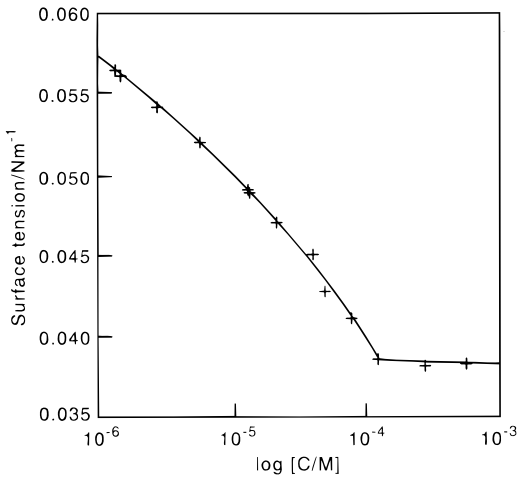

Figure 1. Surface tension of $C_{12}E_{12}$ at the air−water interface as a function of surfactant concentration at 25 °C. The cmc was found to be $(1.25 \pm 0.2) \times 10^{-4}$ M and the limiting area per molecule 78 ± 10 Å^2.

of the surface tension data below the cmc using the Gibbs equation leads to surface excesses in reasonable agreement with those from neutron reflection within a 10% error. Thus, at the cmc neutron reflection produces an area per molecule of 72 ± 3 Å^2 compared with that of 78 ± 10 Å^2 from surface tension measurements using the Gibbs equation. As discussed elsewhere,[18] such agreement is a very good indication that the surfactants are pure. The accuracy of the surface excesses derived from surface tension measurements could be improved by measuring more points below the cmc over a wider tension range.

In neutron reflection the surface excess is most simply determined by measuring the reflectivity from the chain deuterated surfactant in NRW. Rearrangement of eq 12 to

$$\ln h_{ii}(\kappa) = 2\ln\Gamma - \sigma^2\kappa^2/8 \tag{14}$$

gives a simple graphical means of determining the surface coverage. Thus, the surface excess is obtained from the intercept of the straight line plot and the thickness of the layer from the slope. Figure 2 shows the plots of $\ln[h_{cc}(\kappa)]$ versus κ^2 at four different concentrations: the cmc, 0.3cmc, 0.13cmc, and 0.033cmc. The corresponding values of Γ were found to be 2.27, 1.73, 1.42, and $(1.15 \pm 0.05) \times 10^{-10}$ mol cm^{-2}. The corresponding areas per molecule were 72, 93, 116, and 145 ± 5 Å^2, and the thicknesses of the layer 20.0, 18.0, 17.0 and 17.0, ± 1 Å, respectively. Although the area per molecule increases by almost a factor of 2 over the range studied, the thickness of the monolayer does not change significantly. It should be noted that the values of the thickness contain a contribution from the E_{12} group, whose scattering length is not zero, and will therefore be larger than the true thickness of the dodecyl chain layer. We will discuss this further below.

Since $C_{12}E_{12}$ has the longest ethoxylate headgroup in the series of $C_{12}E_n$ so far studied, it is interesting to examine the pattern of the change of surface excess with the size of the headgroup. Figure 3 summarizes the variation of surface excess with concentration for different monodisperse $C_{12}E_n$. We note in passing that the surface coverages in Figure 3 are from neutron reflection and are therefore more accurate than from the less direct surface tension method. They also extend through the cmc in some cases. We also note that for $C_{12}E_n$ where $n =$ 2, 3, and 4 the aggregation above the cmc leads to the formation of liquid crystalline structure rather than discrete micelles. Thus the aggregation concentration should strictly be called critical

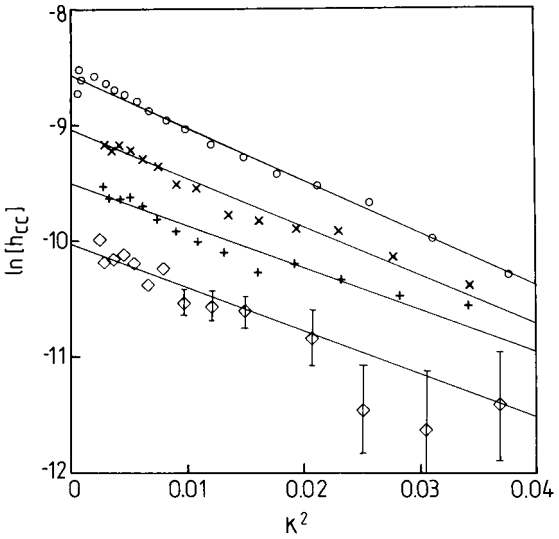

Figure 2. Plots of ln[h_{cc}] versus κ^2 for $dC_{12}hE_{12}$ at the cmc (○), 0.3cmc (×), 0.13cmc (+), and 0.033cmc (◇). The continuous lines are calculated using eq 14 with σ_c = 20.0, 18, 17, and 17 ± 3 Å, respectively. The values of σ_c contain contributions from the hydrogenated heads.

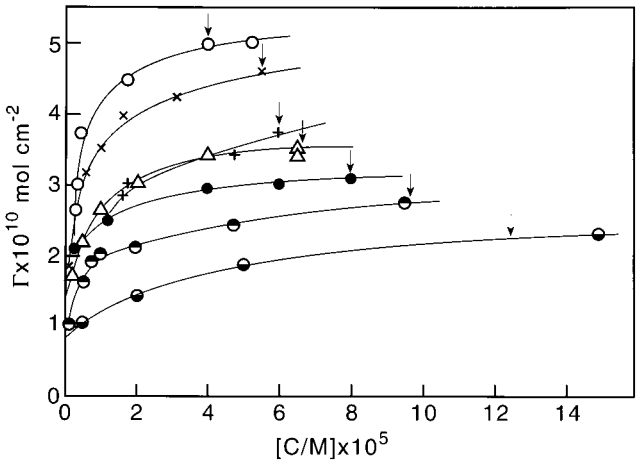

Figure 3. Surface excesses of different $C_{12}E_n$ as a function of concentration determined by neutron reflection, where n = 2 (○), 3 (×), 4 (+), 5 (◇), 6 (●), 8 (◓), and 12 (◒). The cmcs are marked with arrows.

aggregational concentration (CAC). One interesting feature of Figure 3 is that the change of surface excess with concentration becomes more gradual as the size of the E_n group increases. The crossover occurring around $C_{12}E_4$ and $C_{12}E_5$ suggests a change in the pattern of the dependence of surface coverage on bulk concentration for the different size of the headgroup. This may be the case, but the difference in area per molecule between the two surfactants at their cmcs is about 4 Å^2, which is only just outside the error. The slower variation of surface coverage with bulk concentration for the higher $C_{12}E_n$ resembles the behavior of poly(ethylene oxide) (PEO), which has both a very gradual variation of surface tension with concentration[19,20] and of surface excess.[21,22] This will be discussed further below. At this stage we just observe from Figure 3 that the limiting surface excess above the cmc decreases with n, confirming that the limiting area per molecule is determined by the size of the headgroups.

For most surfactants it is relatively easy to label separately the alkyl chain, the head, and the whole molecule so that the full set of six partial structure factors in eq 6 can be determined directly. Preparation of the fully deuterated E_{12} group would be relatively straightforward, but the subsequent purification to obtain a monodisperse compound would not be so easy. However, a limited set of reflectivity profiles may still contain sufficient information for it to be possible to extract the structural parameters, provided that an appropriate combination of contrasts is chosen.[16] Although the hydrogenated E_{12} group in NRW does not give much of a reflected signal, the reflectivity from D_2O solutions is very sensitive to the structure of this group. Because the scattering length density for an E_n group is only slightly greater than zero and because there is a relatively high concentration of E_n in the headgroup region, penetration of D_2O into the headgroup results in a scattering length density about half that of pure D_2O, which is in the range where the reflectivity is very sensitive to the exact composition of this layer. Under these circumstances the reflectivities of deuterated surfactant in NRW and in D_2O and of hydrogenated surfactant in D_2O should be sufficient to define the structure. The sensitivity of the measurement to this layer can be seen from Figure 4 where the reflectivity profiles of the deuterated surfactant and hydrogenated surfactants in D_2O at the cmc are quite different.

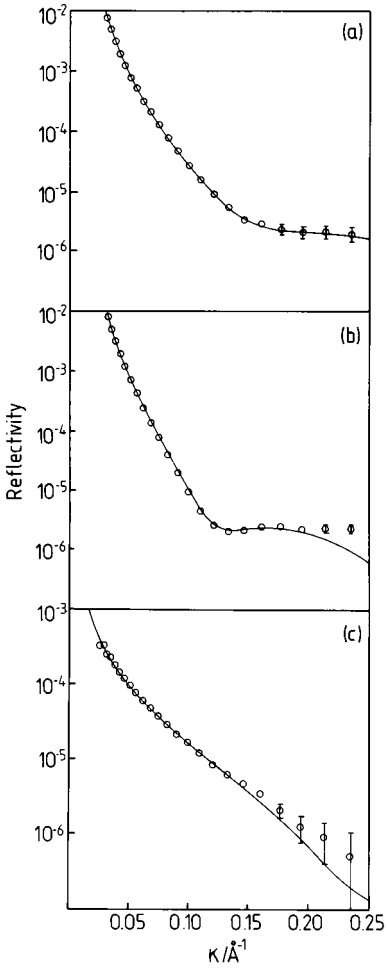

Figure 4. Two-layer model fits to the reflectivity profiles at the cmc: (a) $hC_{12}hE_{12}$ in D_2O; (b) $dC_{12}hE_{12}$ in D_2O; (c) $dC_{12}hE_{12}$ in NRW. Structural parameters used for the calculated reflectivities are given in Table 1.

The reflectivity profiles have been fitted using both the optical matrix method and the kinematic approximation. In using the optical matrix method, the interfacial monolayer was taken to consist of two uniform layers analogous to the model used for other $C_{12}E_n$ with shorter n. The upper layer consists of the dodecyl chain and air. The bottom layer consists of the ethoxylate headgroup and a small fraction of dodecyl chain with the rest of the space filled with water. To apply the two-layer

TABLE 1: Structural Parameters Obtained from Fitting a Two-Layer Model

c/M	isotope	A/Å^2	$\tau_1 \pm 2$/Å	$\tau_2 \pm 2$/Å	chain fraction ± 0.05	no. water
cmc	$dC_{12}hE_{12}$/NRW	72 ± 3	9	15 ± 8	0.35	
	$dC_{12}hE_{12}/D_2O$	72 ± 3	9	22	0.35	26 ± 3
	$hC_{12}hE_{12}/D_2O$	72 ± 3	9 ± 5	22	0.35	25 ± 3
0.3cmc	$dC_{12}hE_{12}$/NRW	93 ± 4	8	13 ± 8	0.38	
	$dC_{12}hE_{12}/D_2O$	93 ± 4	8	21	0.38	30 ± 5
	$hC_{12}hE_{12}/D_2O$	93 ± 4	8 ± 4	21	0.38	30 ± 5
0.13cmc	$dC_{12}hE_{12}$/NRW	116 ± 5	7	13 ± 8	0.44	
	$dC_{12}hE_{12}/D_2O$	116 ± 5	7	20	0.44	40 ± 5
	$hC_{12}hE_{12}/D_2O$	116 ± 5	7 ± 3	20	0.44	40 ± 5
0.033cmc	$dC_{12}hE_{12}$/NRW	145 ± 5	6	12 ± 6	0.50 ± 0.10	
	$dC_{12}hE_{12}/D_2O$	145 ± 5	6	20	0.50 ± 0.10	60 ± 6
	$hC_{12}hE_{12}/D_2O$	145 ± 5	6 ± 3	20	0.50 ± 0.10	60 ± 6

model, it is necessary to assume values for the volumes and fully extended lengths of the dodecyl chain and ethoxylate headgroups. Following Tanford,[23] the volume of the dodecyl chain was taken to be 350 Å^2 with a fully extended length of 16.7 Å. The volume and fully extended length for $(OC_2H_4)_{12}$-OH were taken from Takahashi et al.[24] to be 780 Å^3 and 42.5 Å respectively. The volume of a water molecule was taken to be 30 Å^3. We also assume that there is no difference in the volumes and fully extended lengths of the hydrogenated and deuterated fragments. The scattering lengths for each fragment were evaluated using scattering lengths from ref 25. Examples of the best fits to the measured reflectivity profiles are given in Figure 4 as continuous lines. The fitted parameters for all four concentrations at different contrasts are given in Table 1. At each concentration three reflectivity profiles were fitted with a single set of structural parameters. The small values of the thickness obtained for the headgroup region in NRW are due to the weak signals of the hydrogenated ethoxylate heads which make little contribution to the reflectivity. In comparison with the two-layer models used previously for shorter $C_{12}E_n$ ($n <$ 8), the division of the layers for $C_{12}E_{12}$ has been taken to be at the position where the headgroup and water end, while for $C_{12}E_6$ this division was taken at a position where there was a significant fraction of ethoxylate headgroup mixed into the dodecyl chain layer inside the top layer. The model used here for $C_{12}E_{12}$ results in an apparently thinner alkyl chain region but a much thicker headgroup region. The reason for using the modified model is that the extent of intermixing between alkyl chains and the ethoxylate headgroup in the middle part of the monolayer increases with the size of the headgroup. This makes it difficult to find a clear division in the middle of the layer. Indeed, the previous model for $C_{12}E_6$ could fit the reflectivity profiles for $C_{12}E_{12}$ over a wide range of thickness of chain and head layers at a given concentration. However, the total thickness was always consistent with that obtained using the present model. We observed a similar, but less pronounced, difficulty in fitting a two-layer model to the monolayer of $C_{12}E_8$ at the air−water interface.[3] The two-layer model fitting therefore suggests that the degree of mixing of alkyl chain with ethoxylate headgroup at the center of the monolayer increases progressively with the size of the headgroup.

The total thickness of $C_{12}E_n$ monolayers increases with the size of the headgroup with values of 22.0, 23.0, 23.0, 24.0, 26.5, 28.0, and 31 ± 2 Å for $C_{12}E_2$, $C_{12}E_3$, $C_{12}E_4$, $C_{12}E_5$, $C_{12}E_6$, $C_{12}E_8$, and $C_{12}E_{12}$, respectively.[3,4,6] These relatively small changes with length of the ethoxylate group, whose extended length increases by 3.6 Å per ethoxylate fragment,[24] are also consistent with significant mixing or disorder inside the monolayer. The more direct approach to the extent of mixing between surfactant and water in the monolayer is via the kinematic approximation. The two parameters defining the alkyl chain partial structure factor, containing a small fraction of contribution from the E_{12} headgroup, have already been determined from Figure 2. The distribution of water across the interface can be approximated using eq 13 and Figure 5 shows the water partial structure factors at surfactant concentrations of cmc and 0.13cmc. The continuous lines shown in Figure 5 are calculated using eq 13, and the derived structural parameters are given in Table 2. The rapid decay of the water partial structure factors in the presence of $C_{12}E_{12}$ shows that the presence of the surfactant has a large effect on the normal water distribution and that the disruption increases with surface coverage. The validity of using a tanh function to represent the distribution of water across the interface will be examined later.

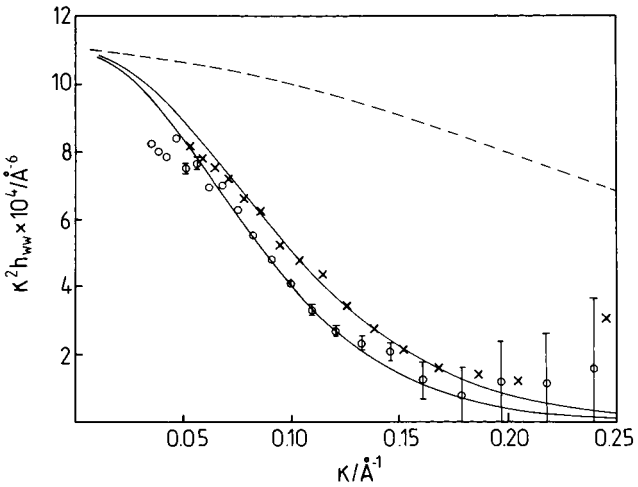

Figure 5. Partial structure factors of the solvent (h_{ww}) versus κ at the cmc (○) and 0.13cmc (×). The continuous lines were calculated using $\xi = 12$ and 10, respectively. The partial structure factor for pure water (dashed line) is shown for comparison.

TABLE 2: Structural Parameters Obtained Using the Kinematic Approximation[a]

	cmc	0.3cmc	0.13cmc	0.033cmc
A/Å^2	72 ± 3	93 ± 4	116 ± 5	145 ± 5
σ_c/Å	20 ± 3	18 ± 3	17 ± 3	17 ± 3
δ_{cw}/Å	13.0 ± 2	11.0 ± 2	10.0 ± 2	7.5 ± 2
ξ_w/Å	12.0 ± 2	11.0 ± 2	10.0 ± 2	9.0 ± 2

[a] σ_c' denotes an apparent chain width because there is a small contribution from the ethylene glycol chain.

The relative distance between the center of the dodecyl chain and water distributions is obtained using eq 10. Figure 6 shows the cross partial structure factors $\kappa^2 h_{cw}$ at four different surfactant concentrations. The separations were found to be 13.0 ± 2 Å at the cmc, decreasing to 7.5 ± 2 Å at the lowest concentration. Although the calculated curves fit the general shape of the measured data well, the fits are poor in the lowest κ range, and this effect is particularly pronounced for the measurement at the cmc. This could result from either unreliability in the measurement of the data at the lowest κ range or inaccuracies

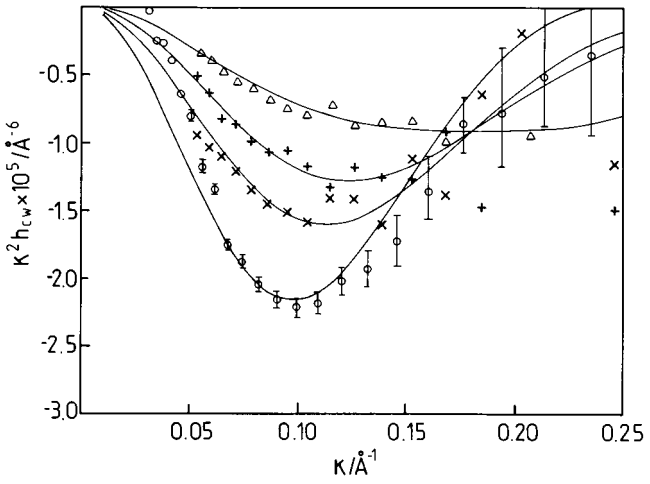

Figure 6. Cross-term partial structure factors at the cmc (○), 0.3cmc (×), 0.13cmc (+) and 0.033cmc (△). The continuous lines were calculated using eq 10 with δ = 13.0, 11.0, 10.0, and 7.5 ± 2 Å, respectively.

in the distributions assumed for different fragments. Unreliability in the calibration of the absolute intensity becomes a problem at very low κ because the demands on the precision of alignment become very large. This is the most probable cause of the discrepancies observed in Figures 5 and 6. It is, however, also possible that the poor fitting could be caused by an inappropriate approximation of the headgroup distribution at large distances in the aqueous solution. Uncertainty in the distribution in this region can affect the reflectivity at very low κ.[21] As discussed previously, this part of the headgroup only occupies a small fraction of the total head volume and will not affect the determination of the cross distance between the center of the alkyl chain and the main part of the headgroup.[21]

The combination of isotopic labels used apparently makes it difficult to obtain direct information about the distribution of the E_{12} group and how it mixes with the water. We have however demonstrated previously[16] that useful information relating to the headgroup can still be derived with good reliability using simultaneous least-squares fitting of the three reflectivity profiles with the analytical expressions for the distributions of three components, eqs 12 and 13, and the relations between the distributions, eqs 9 and 10. These equations lead to five unknown adjustable parameters, the thicknesses of the alkyl chain and E_{12} head, the width parameter for the water distribution, and the distances between chain and head distributions and between chain and water. Figure 7 shows the least-squares fits to the reflectivities at the cmc and 0.13cmc. The parameters obtained are given in Table 3. The derived values of δ_{cw} and ξ are consistent with the kinematic analysis to within an error of 2 Å. The values for δ_{ch} are on average identical with those of the corresponding δ_{cw}, suggesting that the center of the E_{12} headgroup is at almost the same position as the center of the water distribution. In the course of the least-squares fitting it was clear that the reflectivities were sensitive to the variation in δ_{ch}, δ_{cw}, ξ, and σ_c but relatively insensitive to σ_h.

The consistency between the use of the two-layer model and the kinematic analysis can be assessed by comparison of the number density distributions of the different fragments. Figure 8 compares the distributions for the alkyl chain, head, and water at the cmc using the two different methods of analysis. The division in the two-layer model has been chosen as the common reference point. There is reasonable agreement in terms of individual fragment distributions and the distances between them. The extent of intermixing of the different fragments can

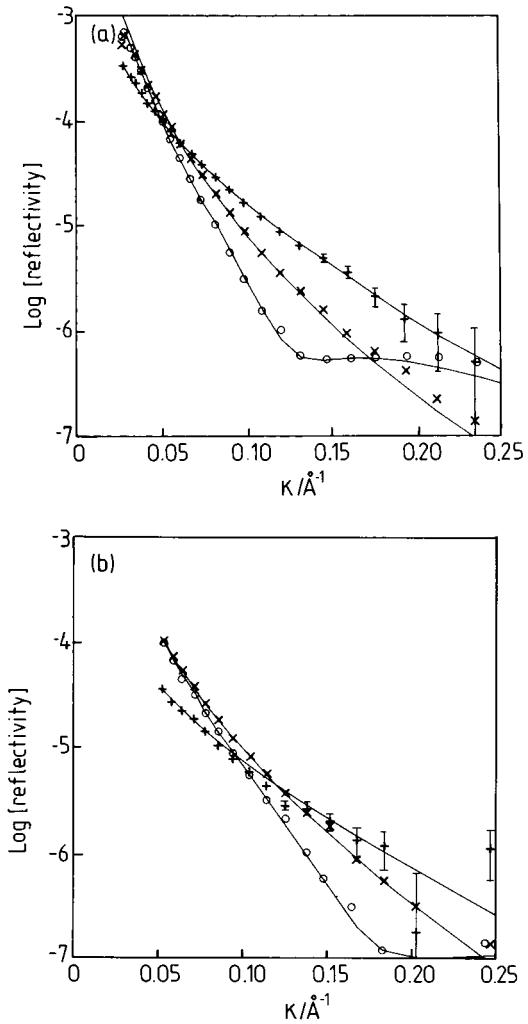

Figure 7. Least-squares fits to the reflectivities at the cmc (a) and 0.13cmc (b): (○) $dC_{12}hE_{12}$ in D_2O; (×) $hC_{12}hE_{12}$ in D_2O; (+) dC_{12}-hE_{12} in NRW. The parameters used for the calculated reflectivities are given in Table 3.

TABLE 3: Structural Parameters Obtained from Least-Squares Fitting to All the Isotopic Data Using the Kinematic Approximation[a]

	cmc	0.3cmc	0.13cmc	0.033cmc
A/Å^2	72 ± 3	93 ± 4	116 ± 5	145 ± 5
σ_c/Å	15 ± 3	13 ± 3	12.5 ± 3	12.0 ± 3
σ_h/Å	21 ± 4	18 ± 4	17 ± 4	17 ± 3
δ_{cw}/Å	13.0 ± 2	11.0 ± 2	10.0 ± 2	7.0 ± 2
δ_{ch}/Å	12.0 ± 2	10.0 ± 2	9.0 ± 2	7.0 ± 2
δ_{hw}/Å	1.5 ± 1	1.0 ± 1	1.0 ± 1	0.0 ± 1
ξ_w/Å	12 ± 2	11 ± 2	10 ± 2	9 ± 2
ω/Å	9.0 ± 1	8.3 ± 1	7.8 ± 1	7.4 ± 1
σ^*_c/Å	12.0	10.0	9.8	9.4
σ^*_h/a	19.0	16.0	15.0	15.3

[a] σ^*_c and σ^*_h were the thicknesses for the alkyl chain and the head after removal of roughness using eq 15.

be examined further by plotting the volume fraction distributions for the whole system, and this is done in Figure 9 for all four concentrations using Gaussian distributions for chain and headgroups and a tanh distribution for water. A further test of self-consistency is that the total volume fraction should be close to unity with a maximum deviation of about ±10%. The overall distributions in Figure 9 largely satisfy this test. It should be noted that both models used to interpret the data assume that the layer is homogeneous in the plane of the surface. However, any inhomogeneity in the surface plane would still have to be

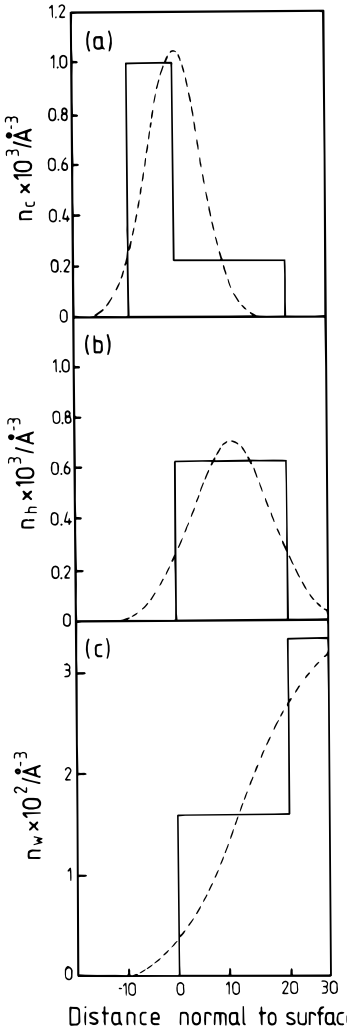

Figure 8. Comparison of the number density distributions normal to the interface of (a) alkyl chain, (b) head, and (c) water at the cmc. The two distributions were calculated from the reflectivity profiles using the optical matrix method (solid lines) and kinematic approximation (dashed lines).

consistent with the average distributions given in the tables and shown in Figures 8 and 9.

As the concentration decreases, the monolayer is immersed further into the aqueous subphase. This has also been observed for other $C_{12}E_n$[3−6] and for a nonionic double-chain sugar surfactant.[26] The extent of mixing between chain and head is clearly seen in Figure 9, and this increases with decreasing concentration, possibly as a result of the extra free space available within the monolayer. The main difference between $C_{12}E_{12}$ and other smaller $C_{12}E_n$ is the decrease of headgroup thickness with surface coverage. For $C_{12}E_3$ the thickness of the headgroup decreases rapidly with concentration while for $C_{12}E_{12}$ the headgroup thickness shows little influence of surface coverage, more like the behavior of a grafted polymer chain, an observation consistent with the simulation results of Sarmoria et al.[9] as will be discussed below. The structural distributions in Figure 9 depend on the intrinsic projection of the fragments onto the surface normal, capillary wave roughness and structural disorder within the layer. We have commented previously that the distributions of surfactant monolayers at the air−water interface are affected by roughness.[3] The relationship between the intrinsic thickness of the surfactant monolayer in the direction normal to the surface (l_z) and the roughness (ω) can be approximately expressed by[7,8]

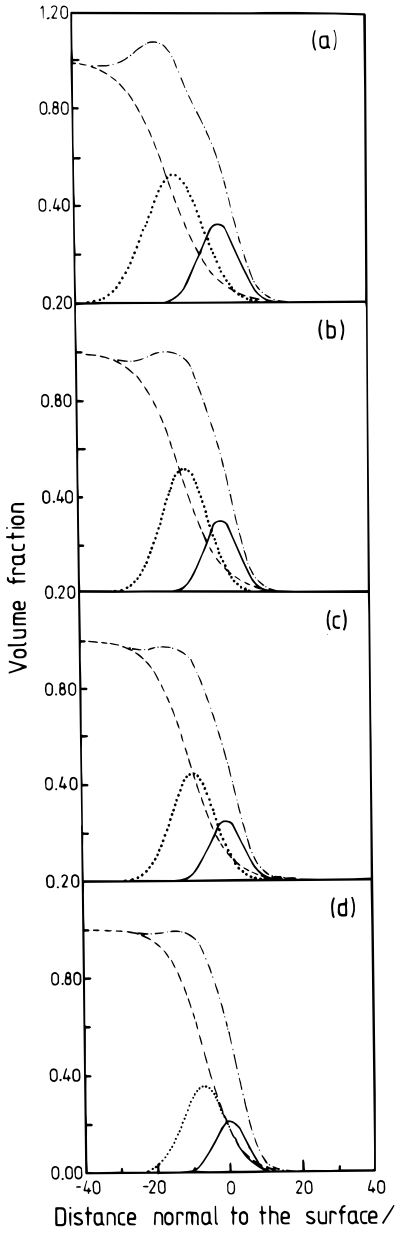

Figure 9. Volume fraction distributions normal to the interface for the whole system and individual fragments at the cmc (a), 0.3cmc (b), 0.13cmc (c), and 0.033cmc (d). The distributions are represented by a solid line for the chain, a dotted line for the head, a dashed line for the water, and a dashed + dotted line for the total.

$$\sigma^2 = l_z^2 + \omega^2 \tag{15}$$

The value of l_z, the intrinsic chain projection, depends on contributions from the extended component lengths, different chain conformations, and the average distribution of orientations with respect to the surface normal. Some of the roughness must originate from capillary waves. The capillary wave amplitude of a pure liquid varies as the square root of surface tension.[27] The level of the contribution of thermal roughness can be similarly estimated from the surface tension. The surface tension of $C_{12}E_{12}$ at its cmc is 38.5 mN m^{-1}, and this will give a capillary wave roughness of about 3.8 Å.[28] Since unit mean square amplitude in terms of capillary waves is equivalent to 2.3 units in terms of the distributions used in the present work, the thermal roughness of 3.8 Å at the cmc is then equivalent to 9 Å in our analysis and will contribute to the broadening of the whole monolayer in the form as described in eq 15.[28] If we remove the value of 9 Å according to eq 15, the projection of

TABLE 4: Structural Parameters for the $C_{12}E_n$ Series at Their cmcs

parameters	$C_{12}E_3$	$C_{12}E_6$	$C_{12}E_8$	$C_{12}E_{12}$
A/Å^2	36 ± 2	55 ± 3	62 ± 3	72 ± 3
σ_c/Å	16.5 ± 2	16.0 ± 2	15.0 ± 2	15.0 ± 3
σ_h/Å	15.5 ± 2	16.5 ± 2	19.0 ± 3	21.5 ± 4
δ_{ch}/Å	8.0 ± 1	9.0 ± 1	10.5 ± 1	12.0 ± 2
δ_{cw}/Å	10.0 ± 1	10.0 ± 1	11 ± 1	13.0 ± 2
ξ_w/Å	6.0 ± 1	8.0 ± 1	9.0 ± 1	12.0 ± 2

the dodecyl chain on the surface normal is estimated to be 12 Å. Since the fully extended length of C_{12} is 16.7 Å this implies that the chains are tilted at angles such that $\langle \cos \theta \rangle = 0.72$. If all the chains are assumed to be at the same angle this would correspond to a tilt of 45° away from the surface normal.

It is interesting to determine the distributions of the ethoxylate group as a function of the number of ethoxylate units and to examine to what extent the in situ headgroup distributions behave like tethered polymer chains. An obvious difference between the adsorbed monolayer at the air−water interface and the true tethered chain at the solid−water interface is the effect of roughness which tends to broaden the width of the monolayer at the air−water interface. Contributions from roughness from different sources will act to form a finite thickness for the wall at the air−water interface, which must be taken into account before comparison with other results. Sarmoria et al.[9] have done simulations on anchored ethoxy groups using the rotational isomeric state model, and these calculations suggest that a polymer-like square root dependence of the extension of the EO units has set in by about $n = 10$. Sarmoria et al.[9] predict an ethylene oxide layer thickness of 18 Å for the grafted E_{12}, which compares reasonably with our value of 19 Å at the cmc after the removal of the contribution of the capillary wave roughness. In their simulation, Sarmoria et al. assumed that there was no significant effect of surface coverage on the distribution of the anchored polymer. Our results show that this is a reasonable assumption for E_{12}, but as can be seen from Figure 3, this is not so for the short E_n. As n decreases, surface coverage is increasingly concentration dependent and so is the layer thickness. Apart from the value of 21 Å at the cmc, the thicknesses at the three lower concentrations are all between 17 and 18 Å. This suggests that the distribution of the ethoxylate head does conform to the prediction of terminally anchored polymer chain behavior. However, it should be emphasized that the accuracy of our current results for the E_{12} fragment would be much improved by performing neutron reflection experiments with head deuterated surfactant.

Conclusions

The extent of overlap between the alkyl chain and the headgroup increases with the size of the ethoxylate group, an observation clearly supported by the values of the parameters listed in Table 4. While the thickness of the dodecyl chain changes very little, the thickness of the headgroup increases substantially with size of the ethoxylate. In parallel, the distance between the centers of the chain and ethoxylate distributions also increases, but not as rapidly as it should if the overlap between chain and head were constant. Conventional wisdom would say that each ethoxylate group is always hydrated with two water molecules, and this would then suggest that increased overlap of the two chains was leading to greater mixing between water and alkyl chain. However, this involves an assumption that there is constant hydration throughout the ethoxylate chain, which is not necessarily the case. It should be remembered that the $C_{12}E_n$ compounds are more soluble in hydrocarbons than in water, and in this case the ethoxylate group is not hydrated at all. The distribution of the headgroups for $C_{12}E_{12}$ agrees well with that predicted by Sarmoria et al., suggesting a tethered polymer-like behavior for the E_{12} group. Indeed, even beyond the limit of the predictions of Sarmoria et al., the whole $C_{12}E_n$ ($n \leq 8$) series shows a reasonable agreement between calculated and observed headgroup distributions, although it should be borne in mind that the calculations assumed that the widths of the distributions were independent of the surface coverage, an assumption which is reasonable for polymeric surfactants but not for $C_{12}E_n$.

Acknowledgment. We thank the Engineering and Physical Science Research Council for support.

References and Notes

(1) Israelachivili, J.; Mitchell, D. J.; Ninham, B. W. *J. Chem. Soc., Faraday Trans. 2* **1976**, *72*, 1525.
(2) Aveyard, R.; Binks, B. P.; Clark, S.; Fletcher, P. D. I. *J. Chem. Soc., Faraday Trans.* **1990**, *86*, 3111.
(3) Lu, J. R.; Li, Z. X.; Thomas, R. K.; Staples, E. J.; Thompson, L.; Tucker, I.; Penfold, J. *J. Phys. Chem.* **1994**, *98*, 6559.
(4) Lu, J. R.; Li, Z. X.; Su, T. J.; Thomas, R. K.; Penfold, J. *Langmuir* **1993**, *9*, 2408.
(5) Lu, J. R.; Hromadova, M.; Simister, E.; Thomas, R. K.; Penfold, J. *J. Phys. Chem.* **1994**, *98*, 11519.
(6) Lu, J. R.; Li, Z. X.; Thomas, R. K.; Staples, E. J.; Tucker, I.; Penfold, J. *J. Phys. Chem.* **1993**, *97*, 8012.
(7) Lu, J. R.; Li, Z. X.; Smallwood, J.; Thomas, R. K.; Penfold, J. *J. Phys. Chem.* **1995**, *99*, 8233.
(8) Lu, J. R.; Li, Z. X.; Thomas, R. K.; Penfold, J. *J. Chem. Soc., Faraday Trans.* **1996**, *92*, 403.
(9) Sarmoria, C.; Blankschtein, D. *J. Phys. Chem.* **1992**, *96*, 1978.
(10) Teo, H. H.; Swales, T. G. E.; Domszy, F.; Heatley, F.; Booth, C. *Makromol. Chem.* **1983**, *184*, 861.
(11) Bucknall, D. G.; Penfold, J.; Webster, J. R. P.; Zarbakhsh, A.; Richardson, R. M.; Rennie, A. R.; Higgins, J. S.; Jones, R.; Fletcher, P. D.; Thomas, R. K.; Roser, S. J., Dickinson, E. Proceedings of International Conference on Advanced Neutron Sources XIII and ESS-PM4 PSI Proceedings 95−02; **1995**, *1*, 123.
(12) Lee, E. M.; Thomas, R. K.; Penfold, J.; Ward, R. C. *J. Phys. Chem.* **1989**, *93*, 381.
(13) Born, M.; Wolf, E. *Principles of Optics*; Pergamon: Oxford, 1970.
(14) Lekner, J. *Theory of Reflection*; Nijhoff: Dordrecht, 1987.
(15) Crowley, T. L. *Physica* **1993**, *A195*, 354.
(16) Lu, J. R.; Lee, E. M.; Thomas, R. K. *Acta Crystallogr.* **1996**, *A52*, 11.
(17) Lange, H. *Kolloid Z.* **1965**, *201*, 131.
(18) An, S. W.; Lu, J. R.; Thomas, R. K.; Penfold, J. *Langmuir* **1996**, *12*, 2446.
(19) Glass, J. E. *J. Phys. Chem.* **1968**, *72*, 4459.
(20) Couper, A., Eley, D. D. *J. Polym. Sci.* **1948**, *3*, 345.
(21) Lu, J. R.; Su, T. J.; Thomas, R. K.; Penfold, J.; Richards, R. W. *Polymer* **1996**, *37*, 109.
(22) Henderson, J. A.; Richards, R. W.; Penfold, J.; Thomas, R. K.; Lu, J. R. *Macromolecules* **1993**, *26*, 4591.
(23) Tanford, C. J. *J. Phys. Chem.* **1972**, *76*, 3020.
(24) Takahashi, Y.; Sumita, I.; Tadokoro, H. *J. Polym. Sci.* **1973**, *11*, 2113.
(25) Sears, V. F. *Neutron News* **1992**, *3*, 26.
(26) Cooke, D. J.; Lu, J. R.; Lee, E. M.; Thomas, R. K., Pitt, A. R.; Simister, E. A.; Penfold, J. *J. Phys. Chem.* **1996**, *100*, 10298.
(27) Schwartz, D. K.; Schlossman, M. L.; Kawamoto, E. H.; Kellogg, G. J.; Pershan, P. S.; Ocko, B. M. *Phys. Rev.* **1990**, *A41*, 5687.
(28) Lu, J. R.; Simister, E. A.; Thomas, R. K.; Penfold, J. *J. Phys.: Condens. Matter* **1994**, *6*, A403.